

# Charged Scalar Perturbations around Garfinkle-Horowitz-Strominger Black Holes

Cheng-Yong Zhang<sup>1\*</sup>, Shao-Jun Zhang<sup>2†</sup>, and Bin Wang<sup>1‡</sup>

<sup>1</sup> Department of Physics and Astronomy, Shanghai Jiao Tong University, Shanghai 200240, China

<sup>2</sup> Instituto de Física, Universidade de São Paulo, C.P. 66318, 05315-970, São Paulo, SP, Brazil

## Abstract

We examine the stability of the Garfinkle-Horowitz-Strominger (GHS) black hole under charged scalar perturbations. We find that different from the neutral scalar field perturbations, only two numerical methods, such as the continued fraction method and the asymptotic iteration method, can keep high efficiency and accuracy requirements in the frequency domain computations. The comparisons of the efficiency between these two methods have also been done. Employing the appropriate numerical method, we show that the GHS black hole is always stable against charged scalar perturbations. This is different from the result obtained in the de Sitter and Anti-de Sitter black holes. Furthermore we argue that in the GHS black hole background there is no amplification of the incident charged scalar wave to cause the superradiance, so that the superradiant instability cannot exist in this spacetime.

PACS numbers: 04.50.Kd, 04.70.-s, 04.25.Nx

## 1 Introduction

Perturbation around black holes has been an intriguing subject of discussions in the past three decades. This is mainly because that the study of black hole perturbations is a powerful tool to disclose the

---

\*zhangcy@sjtu.edu.cn

†sjzhang84@hotmail.edu.cn

‡wang\_b@sjtu.edu.cn

stability of the black hole spacetime. If the black hole is unstable against small perturbations, it will inevitably disappear or transform dynamically into another object. Stability analysis of (3+1)-dimensional asymptotically flat black holes, such as Schwarzschild, Reissner-Nordstrom (RN) and Kerr black holes, has been studied thoroughly against different kinds of perturbations including neutral scalar, electromagnetic and gravitational perturbations and all these black holes were found stable. Considering that our universe may have a small positive cosmological constant, the perturbation analysis has been extended to (3+1)-dimensional Schwarzschild-de Sitter (dS), RN-dS, and Kerr-dS black holes and evidences for the stability of these more possible astrophysical black holes have been reported. Recently, motivated by the discovery of the correspondence between physics in the anti-de Sitter (AdS) spacetime and conformal field theory (CFT) on its boundary (AdS/CFT), the perturbations around four-dimensional AdS black holes have been examined and (3+1)-dimensional AdS black holes were found stable under neutral scalar, electromagnetic and gravitational perturbations. It was concluded that all of the considered four-dimensional black holes tested for stability are stable, except the string theory generalization of Kerr-Newman black holes whose stabilities have not been tested due to the difficulty in decoupling the angular variables in their perturbation equations. For a review on this topic, see [1, 2] for example and references therein.

Recently, the exploration of the black hole spacetime stability has been extended to examine the perturbation against the charged scalar field. In the AdS spacetime, it was first observed that the (3+1)-dimensional RN-AdS black hole can be destroyed and the four-dimensional AdS hole can become unstable due to the condensation of the charged scalar hair onto the black hole. The (3+1)-dimensional RN-AdS black hole will finally be transformed into another new hairy black hole under the small charged scalar field perturbation [3, 4, 5], see review for example [6]. It would be interesting to ask whether the observed instability only happens for the AdS black holes because of their special spacetime properties, whether such dynamical instability can also appear in other four-dimensional black hole backgrounds. In [7], a new instability in the four-dimensional RN-dS black holes against charged scalar perturbations was disclosed. This result was later confirmed in [8]. Can this instability be a general property? In this paper, we would like to examine this problem further. We will extend the discussion of the charged scalar perturbation to the (3+1)-dimensional dilaton black hole obtained by Garfinkle, Horowitz and Strominger [9](GHS) from the low energy effective action in string theory. Its limiting case reduces to the four-dimensional Schwarzschild black hole, see review [10]. The stability of this dilaton black hole has been proved by examining the perturbation against neutral scalar fields [11, 12, 13]. Here we are going to test the stability of such black hole against charged scalar perturbation and try to answer whether the instability observed for the charged scalar perturbation can also happen in this stringy four-dimensional black hole background and its limiting

Schwarzschild spacetime.

We will concentrate on the frequency domain studies of the charged scalar perturbation around the stringy black hole. It is important to calculate the frequency of perturbations with very high accuracy because considerable changing of black hole parameters frequently changes perturbation frequency just by a few percent. With the nonzero charge of the scalar field, we will explain that not all available numerical methods for solving the eigenvalue problem of the perturbation can keep high accuracy. The continued fraction method (CFM) [14, 15] and the asymptotic iteration method (AIM) [16, 17, 18] still win the accuracy and efficiency competition against the other numerical methods. The CFM method was argued as the most accurate in calculating the frequency of the perturbation [19]. Although this still holds when the charge of the scalar field is low, we will show that its accuracy and efficiency will be decreased and lower than that of the AIM method when the scalar field is heavily charged. Further comparison of the accuracy and efficiency of numerical methods in calculating the frequency of the perturbation is important, because this can help to choose the right numerical tool in obtaining the real physics on the stability of the black hole.

The organization of the paper is as follows. In Sec.2 we will introduce the background spacetime of the stringy black hole and derive the equation of motion for charged scalar perturbations. In Sec.3, we will first review the CFM and AIM methods for numerical computations of the frequency of the perturbation. Then we will compare the efficiency and accuracy of these two methods and also with other methods. In the following section, we will give numerical results on the frequency of the charged scalar perturbations. We will present our summaries and discussions in the final section.

## 2 The GHS black hole and equation of charged scalar perturbation

The GHS black hole is a solution obtained from the low energy effective action in string theory by dropping all the fields except the metric  $g_{\mu\nu}$ , a dilaton  $\phi$  and a Maxwell field  $F_{\mu\nu}$ . In string frame, the action is [20]

$$W = \frac{1}{16\pi} \int d^4x \sqrt{-g} e^{-2\phi} [R + 4(\nabla\phi)^2 - F_{\mu\nu}F^{\mu\nu}] - \frac{1}{2} g^{\mu\nu} \bar{D}_\mu \bar{\psi} D_\nu \psi - V(\psi, \bar{\psi}), \quad (1)$$

where we have added the perturbing charged scalar field  $\psi$  to study its perturbation on the background of the GHS black hole. Here  $\bar{D}_\mu \bar{\psi} D_\nu \psi \equiv (\partial_\mu + iqA_\mu) \bar{\psi} (\partial_\nu - iqA_\nu) \psi$  with  $q$  being the charge of the scalar field  $\psi$ .  $V(\psi, \bar{\psi})$  is the potential of the perturbing charged scalar field. Its usual form is taken as  $V(\psi, \bar{\psi}) = \frac{1}{2} \mu^2 \psi \bar{\psi} + \frac{\lambda}{4} (\psi \bar{\psi})^2$ , in which  $\mu$  is the mass of the scalar field  $\psi$  and the  $\lambda$  term represents the self-interaction of  $\psi$ . We set  $\lambda = 0$  hereafter for simplicity. This action can be viewed as a special

case in scalar-tensor theory [21] with  $F(\phi) = e^{-2\phi}$  and  $Z(\phi) = -4e^{-2\phi}$ .

Doing a conformal transformation  $g_{\mu\nu}^E = e^{-2\phi}g_{\mu\nu}$ , the action can be rewritten in the Einstein frame as

$$W = \frac{1}{16\pi} \int d^4x \sqrt{-g_E} [R_E - 2(\nabla\phi)^2 - e^{-2\phi}F_{\mu\nu}F^{\mu\nu}] - \frac{1}{2}e^{2\phi}g_E^{\mu\nu}\bar{D}_\mu\bar{\psi}D_\nu\psi - e^{4\phi}V(\psi, \bar{\psi}). \quad (2)$$

At the first sight, it seems difficult to find the exact background solution to equations of motion derived from the action Eq. (2) (The background solution means the solution not taking into account the back-reaction of the perturbing field  $\psi$ ). However, the symmetry property of this action allows one to obtain a one-parameter family of solutions [9, 10, 22],

$$ds_E^2 = -\left(1 - \frac{2M}{r}\right) dt^2 + \left(1 - \frac{2M}{r}\right)^{-1} dr^2 + r\left(r - \frac{Q^2}{M}\right) d\Omega^2. \quad (3)$$

This is the well-known Garfinkle-Horowitz-Strominger (GHS) black hole. Here  $d\Omega^2 = d\theta^2 + \sin^2\theta d\varphi^2$ .  $M$  is the physical mass and  $Q$  the physical charge of the GHS black hole. The electric field and the background dilaton field are

$$A_t = -\frac{Q}{r}, \quad F_{rt} = \frac{Q}{r^2}, \quad e^{2\phi} = 1 - \frac{Q^2}{Mr}. \quad (4)$$

It is obvious that the electric charge and the dilaton are not independent. The GHS solution reduces to the Schwarzschild black hole in the limit  $Q \rightarrow 0$ .

In the limit  $Q \rightarrow 0$ , the area of the sphere  $r = Q^2/M$  is zero so that this surface is singular. When  $Q^2 < 2M^2$ , this singular surface is surrounded by the event horizon  $r = 2M$ . As one increases  $Q$ , the singular surface can coincide with the horizon when  $Q^2 = 2M^2$  and even moves outside the horizon and becomes timelike if  $Q^2 > 2M^2$ . In our paper, we will consider the case when  $Q^2 < 2M^2$ .

Ignoring the self-interaction term, the equation of motion of the perturbing charged scalar field is

$$\left(g_E^{\mu\nu}D_\mu D_\nu - \mu^2 e^{2\phi}\right)\psi = 0. \quad (5)$$

Here  $\mu^2 e^{2\phi}$  plays the role of the effective mass square of  $\psi$ . Since the background spacetime is spherical symmetry, we can separate the radial and angular part of  $\psi$ . Using the ansatz  $\psi = e^{-i\omega t} \frac{\Psi(r)}{\sqrt{r^2 - \frac{Q^2}{M}r}} Y(\theta, \varphi)$  and introducing the tortoise coordinate  $dr = \left(1 - \frac{2M}{r}\right) dr_*$ , we get the radial

part of the perturbation equation

$$\frac{\partial^2 \Psi}{\partial r_*^2} + \left[ \left( \omega - \frac{qQ}{r} \right)^2 - V \right] \Psi = 0 \quad (6)$$

in which

$$\begin{aligned} V = & -\frac{3}{4} \frac{\left(2r - \frac{Q^2}{M}\right)^2 (r - 2M)^2}{r^4 \left(r - \frac{Q^2}{M}\right)^2} + \frac{(r - 2M)^2}{r^3 \left(r - \frac{Q^2}{M}\right)} + \frac{\left(2r - \frac{Q^2}{M} - 2M\right) \left(2r - \frac{Q^2}{M}\right) (r - 2M)}{2 \left(r - \frac{Q^2}{M}\right)^2 r^3} \\ & + \frac{\left(r - \frac{Q^2}{M}\right) (r - 2M)}{r^2} \mu^2 + \frac{l(l+1) (r - 2M)}{\left(r - \frac{Q^2}{M}\right) r^2} \end{aligned} \quad (7)$$

and the effective potential  $V_{eff} = V - \frac{q^2 Q^2}{r^2}$ . Here  $l$  is the spherical harmonic index. It can be shown that we always have  $V > 0$  when  $r > 2M$  and  $Q^2 < 2M^2$ .

### 3 Numerical methods

A practical tool for testing stability of black holes is the numerical investigation of the perturbations around black hole backgrounds. Usually considerable changing of black hole parameters results in the change of just a few percent in the frequency of the perturbation. Thus the high accuracy of the computation is the key factor in examining the perturbation around black holes. Meanwhile the efficiency of the computation is also an important factor in solving the perturbation equations numerically.

In this work, we will concentrate on the frequency domain to disclose the property of the perturbation. We will refine different numerical methods and try to solve the eigenvalue problem of the perturbation equation with high accuracy and efficiency. Comparing with other numerical methods, we find that the CFM and AIM methods can meet requirements of the high accuracy and efficiency in the computation. We will first review these two methods. Furthermore we will show that in different parameter ranges, the accuracy and efficiency also differ between these two refined methods. Without loss of generality, we will set  $M = 1$  and  $\mu = 0$  in the following discussions.

### 3.1 Continued fraction method

The CFM was proposed by Leaver [14] when he calculated the quasinormal modes (QNMs) of the Kerr black hole and is considered as the most accurate method to calculate the frequencies of perturbations [19]. The core of this method is to cast the perturbation equation into a three-term recurrence relation, and from it we can get a continued fraction equation characterizing the perturbations. The CFM is thought to be able to give frequencies of perturbations with high numerical precision as there is no intermediate approximation compared to other numerical methods. See reviews [1, 19] for more details. In this subsection, we try to get the three-term recurrence relation and the corresponding continued fraction equation.

To calculate the frequency, we start from the physical boundary conditions which can be derived by studying the asymptotic behavior of Eq. (6)

$$\Psi \sim \begin{cases} e^{-i(\omega - \frac{qQ}{2M})r_*}, & r_* \rightarrow -\infty (r \rightarrow 2M), \\ e^{i\sqrt{\omega^2 - \mu^2}r_*}, & r_* \rightarrow \infty (r \rightarrow \infty), \end{cases} \quad (8)$$

which means that there only exists the ingoing wave at the event horizon and the outgoing wave at the infinity.

A solution to the radial equation Eq. (6) encoding the above boundary conditions can be written in the form as

$$\Psi = \left(\frac{r}{2M} - 1\right)^{-i(2M\omega - qQ)} \left(\frac{r}{2M}\right)^{i2M(\omega + \sqrt{\omega^2 - \mu^2} - \frac{qQ}{2M})} e^{i\sqrt{\omega^2 - \mu^2}(r - 2M)} \sum_{n=0}^{\infty} a_n x^n, \quad (9)$$

in which  $x = \frac{r-2M}{r}$  and  $a_0 = 1$ . Substituting this expansion into the radial equation (6), we get a six-term recurrence relation.

$$\begin{aligned} \beta_0 a_0 + \alpha_0 a_1 &= 0, \\ \gamma_1 a_0 + \beta_1 a_1 + \alpha_1 a_2 &= 0, \\ \delta_2 a_0 + \gamma_2 a_1 + \beta_2 a_2 + \alpha_2 a_3 &= 0, \\ \eta_3 a_0 + \delta_3 a_1 + \gamma_3 a_2 + \beta_3 a_3 + \alpha_3 a_4 &= 0, \\ \theta_4 a_0 + \eta_4 a_1 + \delta_4 a_2 + \gamma_4 a_3 + \beta_4 a_4 + \alpha_4 a_5 &= 0, \\ \theta_n a_{n-4} + \eta_n a_{n-3} + \delta_n a_{n-2} + \gamma_n a_{n-1} + \beta_n a_n + \alpha_n a_{n+1} &= 0, \end{aligned} \quad (10)$$

where the recurrence coefficients are given by

$$\begin{aligned}
\alpha_n &= (Q^2 - 2)^2 [-4n^2 - 8(1 + iqQ - 2i\omega)n - 4(1 + 2iqQ) + 16i\omega], \\
\beta_n &= 2(Q^2 - 2) [2n^2(5Q^2 - 6) + 4n(-2 + iqQ(5Q^2 - 6) + Q^2(1 - 14i\omega) + 20i\omega)] \\
&\quad + 2(Q^2 - 2) [-4 - 4l(l + 1) + Q^2 + 4qQ(i - qQ)(Q^2 - 2)] \\
&\quad + 2(Q^2 - 2) [8(5qQ - 2i)(Q^2 - 2)\omega - 64(Q^2 - 2)\omega^2],
\end{aligned} \tag{11}$$

$$\begin{aligned}
\gamma_n &= -8n^2(5Q^4 - 12Q^2 + 6) + 16l(l + 1)(Q^2 - 1) \\
&\quad - 16 + 36Q^2 - 17Q^4 + 16iqQ(2 - 6Q^2 + 3Q^4) + 4q^2Q^2(12 - 20Q^2 + 7Q^4) \\
&\quad - 16[i(8 - 20Q^2 + 9Q^4) + 4qQ(6 - 11Q^2 + 4Q^4)]\omega + 64(12 - 20Q^2 + 7Q^4)\omega^2 \\
&\quad - 16in[2i + qQ(6 - 12Q^2 + 5Q^4) + Q^4(3i - 17\omega) - 24\omega + Q^2(44\omega - 6i)], \\
\delta_n &= 8n^2(2 - 8Q^2 + 5Q^4) - 8l(l + 1)Q^2 \\
&\quad + 16 - 100Q^2 + 79Q^4 - 16iqQ(2 - 10Q^2 + 7Q^4) - 4q^2Q^2(4 - 16Q^2 + 9Q^4) \\
&\quad + 16[2i(4 - 20Q^2 + 13Q^4) + qQ(8 - 32Q^2 + 19Q^4)]\omega - 64(4 - 16Q^2 + 9Q^4)\omega^2 \\
&\quad + 16in[2i + qQ(2 - 8Q^2 + 5Q^4) + Q^4(7i - 19\omega) - 8\omega + 2Q^2(16\omega - 5i)],
\end{aligned} \tag{12}$$

$$\begin{aligned}
\eta_n &= Q^2 [-4n^2(5Q^2 - 4) + 4q^2Q^2(5Q^2 - 4)] \\
&\quad + 8nQ^2 [-8 - iqQ(5Q^2 - 4) + Q^2(11 + 20i\omega) - 16i\omega] \\
&\quad + Q^2(-5i + 8\omega)[12i - 32\omega + Q^2(-19i + 40\omega)] \\
&\quad + 8qQ^3[8i - 16\omega + Q^2(-11i + 20\omega)], \\
\theta_n &= Q^4 [4n^2 + 8in(3i + qQ - 4\omega) + 35 - 4q^2Q^2 + 96i\omega - 64\omega^2 + 8qQ(-3i + 4\omega)].
\end{aligned} \tag{13}$$

We can use the Gauss elimination to reduce the six-term recurrence relation to a five-term recurrence relation,

$$\begin{aligned}
\beta'_0 &= \beta_0, \gamma'_1 = \gamma_1, \beta'_1 = \beta_1, \quad \delta'_2 = \delta_2, \gamma'_2 = \gamma_2, \beta'_2 = \beta_2, \\
\eta'_3 &= \eta_3, \delta'_3 = \delta_3, \gamma'_3 = \gamma_3, \quad \beta'_3 = \beta_3, \alpha'_n = \alpha_n (n \geq 0), \\
\eta'_n &= \eta_n - \frac{\theta_n}{\eta'_{n-1}} \delta'_{n-1}, \quad \delta'_n = \delta_n - \frac{\theta_n}{\eta'_{n-1}} \gamma'_{n-1} (n \geq 4), \\
\gamma'_n &= \gamma_n - \frac{\theta_n}{\eta'_{n-1}} \beta'_{n-1}, \quad \beta'_n = \beta_n - \frac{\theta_n}{\eta'_{n-1}} \alpha'_{n-1} (n \geq 4).
\end{aligned} \tag{14}$$

By repeating the Gauss elimination, a four-term recurrence relation can be derived,

$$\begin{aligned}\beta_0'' &= \beta_0', \gamma_1'' = \gamma_1' \quad , \quad \beta_1'' = \beta_1', \\ \delta_2'' &= \delta_2', \gamma_2'' = \gamma_2', \beta_2'' = \beta_2' \quad , \quad \alpha_n'' = \alpha_n' (n \geq 0), \\ \delta_n'' &= \delta_n' - \frac{\eta_n'}{\delta_{n-1}''} \gamma_{n-1}'', \gamma_n'' = \gamma_n' - \frac{\eta_n'}{\delta_{n-1}''} \beta_{n-1}'' \quad , \quad \beta_n'' = \beta_n' - \frac{\eta_n'}{\delta_{n-1}''} \alpha_{n-1}'' (n \geq 3).\end{aligned}\tag{15}$$

And at last we get a three-term recurrence relation

$$\begin{aligned}\beta_0''' &= \beta_0'', \gamma_1''' = \gamma_1'' \quad , \quad \beta_1''' = \beta_1'', \alpha_n''' = \alpha_n'' (n \geq 0), \\ \gamma_n''' &= \gamma_n'' - \frac{\delta_n''}{\gamma_{n-1}'''} \beta_{n-1}''' \quad , \quad \beta_n''' = \beta_n'' - \frac{\delta_n''}{\gamma_{n-1}'''} \alpha_{n-1}''' (n \geq 2).\end{aligned}\tag{16}$$

Then the frequencies of the perturbations are the solutions to the characteristic continued fraction equation

$$0 = \beta_0''' - \frac{\alpha_0''' \gamma_1'''}{\beta_1''' - \frac{\alpha_1''' \gamma_2'''}{\beta_2''' - \frac{\alpha_2''' \gamma_3'''}{\beta_3''' - \dots}}}.\tag{17}$$

It is obvious that the six-term recurrence relation reduces to a four-term recurrence relation when  $Q = 0$  or  $Q = \sqrt{2}$  due to the vanish of some coefficients in (12). When  $Q = 0$ , the GHS metric reduces to the Schwarzschild metric, and the six-term recurrence relation boils down to a four-term recurrence relation which later coincides with the three-term recurrence relation derived in ref. [14] after doing the Gauss elimination with  $2M = 1$ .

### 3.2 Asymptotic iteration method

The asymptotic iteration method (AIM) was first used to solve the eigenvalue problems of second order homogeneous linear differential equations [16]. It was then applied to find the frequencies of perturbations in Schwarzschild and Schwarzschild (anti-) de Sitter black holes [17]. See review [18] and references therein.

Let's consider a second order homogeneous linear differential equations

$$\chi'' = \lambda_0(x)\chi' + s_0(x)\chi,\tag{18}$$

where  $\lambda_0(x)$  and  $s_0(x)$  are smooth functions in some interval  $[a, b]$ . Differentiating it with respect to  $x$ , we get

$$\chi''' = \lambda_1(x)\chi' + s_1(x)\chi,\tag{19}$$



where

$$\lambda_1(x) = \lambda'_0(x) + s_0(x) + (\lambda_0(x))^2, \quad s_1 = s'_0(x) + s_0(x)\lambda_0(x). \quad (20)$$

Using this step iteratively, we can get the  $(n+2)$ th derivatives

$$\chi^{(n+2)} = \lambda_n(x)\chi' + s_n(x)\chi \quad (21)$$

where

$$\lambda_n(x) = \lambda'_{n-1}(x) + s_{n-1}(x) + \lambda_0(x)\lambda_{n-1}(x), \quad s_n(x) = s'_{n-1}(x) + s_0(x)\lambda_{n-1}(x). \quad (22)$$

For sufficiently large  $n$ , the asymptotic aspect of the method was introduced [18],

$$\frac{s_n(x)}{\lambda_n(x)} = \frac{s_{n-1}(x)}{\lambda_{n-1}(x)} \quad (23)$$

which is equivalent to imposing a termination to the number of iterations [23]. The perturbation frequencies can be derived from this “quantization condition”. However, the derivatives of  $\lambda_n(x)$  and  $s_n(x)$  in each iteration slow down the AIM considerably and also lead to precision problems. These drawbacks were overcome in ref. [17]. One can expand  $\lambda_n(x)$  and  $s_n(x)$  in Taylor series around a regular point  $\xi$  at which the AIM is performed,

$$\lambda_n(\xi) = \sum_{i=0}^{\infty} c_n^i (x - \xi)^i, \quad s_n(x) = \sum_{i=0}^{\infty} d_n^i (x - \xi)^i. \quad (24)$$

Here  $c_n^i$  and  $d_n^i$  are the  $i$ th Taylor coefficients of  $\lambda_n(\xi)$  and  $s_n(\xi)$ , respectively. Substituting these expansions into (22), we get a set of recursion relations for the coefficients,

$$c_n^i = (i+1)c_{n-1}^{i+1} + d_{n-1}^i + \sum_{k=0}^i c_0^k c_{n-1}^{i-k}, \quad d_n^i = (i+1)d_{n-1}^{i+1} + \sum_{k=0}^i d_0^k c_{n-1}^{i-k}. \quad (25)$$

The quantization condition then can be expressed as

$$d_n^0 c_{n-1}^0 - d_{n-1}^0 c_n^0 = 0, \quad (26)$$

which will give us the perturbation frequencies of a black hole. Both the accuracy and efficiency of AIM are greatly improved with this expansion [17].

Now we apply this method to the GHS black hole. Taking a coordinate transformation  $x = 1 - \frac{2M}{r}$

and an abbreviation  $a = \frac{Q^2}{2M^2}$ , the perturbation equation (6) turns into the standard form as Eq. (18)

$$\frac{\partial^2 \Psi}{\partial x^2} = \lambda_0(x) \frac{\partial \Psi}{\partial x} + s_0(x) \Psi \quad (27)$$

in which

$$\begin{aligned} \lambda_0(x) &= \frac{3x-1}{x(1-x)}, \\ s_0(x) &= \frac{-1}{x^2(1-x)^2} \left[ \frac{3}{4} \left( \frac{2-a+ax}{1-a+ax} \right)^2 x^2 - \frac{x^2}{1-a+ax} - \frac{1}{2} \left( \frac{1-a+(a+1)x}{1-a+ax} \right) \left( \frac{2-a+ax}{1-a+ax} \right) x \right] \\ &\quad - \frac{1}{x^2(1-x)^2} \left[ \left( \frac{2M\omega}{1-x} - qQ \right)^2 - (1-a+ax) \frac{4M^2x}{(1-x)^2} \mu^2 - \frac{l(l+1)x}{(1-a+ax)} \right]. \end{aligned} \quad (28)$$

Now the infinity corresponds to  $x \rightarrow 1$  and the horizon is at  $x \rightarrow 0$ . We can choose the regular point  $\xi$  between 0 and 1. Substituting (28) into the (24) (25) (26), we can get frequencies of perturbations around the GHS black hole.

As we can see from (24), the efficiency and accuracy of the numerical result depend on the position of the expansion  $\xi$ . In our calculation, we find that when the charge of the black hole is not too large, the position of the expansion point has little influence and the AIM converges well. However, when the charge of the black hole is larger than  $M$ , the position of expansion will affect the efficiency and accuracy of the numerical computation apparently.

### 3.3 The efficiency and accuracy comparisons between AIM and CFM

In this subsection, we present the efficiency and accuracy comparisons between two numerical methods, the CFM and the AIM. The reason for us to concentrate on these two numerical methods in doing computation is that we have found that other numerical methods, such as the shooting method [24, 25], the WKB method [26, 27, 28] and the finite difference method [29, 30, 31] cannot give us good convergence and reliability in the computation when the scalar field is charged, although they can give consistent frequencies for the neutral scalar perturbations. In our numerical computations we have set  $M = 1$  and  $\mu = 0$ .

For the fundamental modes of the charged scalar perturbation, it is easy to see that both methods, the AIM and the CFM, are easy to converge. For example as shown in Table 1, when  $l = 1, Q = 0.5$  and  $q = 1$ , only 20 iterative steps are needed for CFM to get the fundamental mode with relative error  $10^{-5}$  compared to the result obtained using 100 iterative steps, and 30 iterative steps for AIM with

relative error  $10^{-4}$  compared to the results obtained by 100 iterative steps, respectively. However, for the overtones, we found that more iterative steps are needed compared to the fundamental modes in order to keep the accuracy. We adopt 100 iterative steps for both AIM and CFM in our numerical calculations.

$l = 1, Q = 0.5, q = 1$	CFM	AIM ( $\xi = 0.45$ )
iterative steps	20	30
fundamental $n = 0$ (relative error with respect to 100 steps)	0.491714-0.111583i (0.0005%,0.0028%)	0.491758-0.111572i (-0.0085%,0.0128%)
overtone $n = 1$ (relative error with respect to 100 steps)	0.479728-0.339701i (0.0194%,-0.0126%)	0.477759-0.339279 (4.2983%,0.1115%)

Table 1: Fundamental mode  $n = 0$  and the first overtone  $n = 1$  when  $l = 1, Q = 0.5$  and  $q = 1$ . The two numbers in brackets are relative errors of the real and imaginary part of the modes compared to the ones calculated with 100 iteration steps, respectively. For the AIM, we do the expansion at the point  $\xi = 0.45$ .

When the charge  $Q$  of the black hole is small, results given by two methods, the CFM and AIM, agree quite well with each other. However, the situation changes when  $Q$  becomes large. We find that for the chosen large value of  $Q$ , the speed of convergence of AIM is faster than that of the CFM when the scalar perturbation field is weakly charged, but when the charge  $q$  of the scalar field increases, the speed of the convergence of the CFM becomes faster than that of the AIM. See Table 2 for concrete examples.

$l = 1, n = 1$		$q = 0.5$	$q = 2$
iterative steps		80 (relative error with respect to 100 steps)	80 (relative error with respect to 100 steps)
$Q = 0.1$	AIM ( $\xi = 0.45$ )	0.28448-0.31036i ( $-4.1 \times 10^{-6}, -3.0 \times 10^{-6}$ )	0.343659-0.321025i ( $-2.7 \times 10^{-6}, -1.4 \times 10^{-7}$ )
	CFM	0.28448-0.31036i ( $-2.1 \times 10^{-7}, 4.0 \times 10^{-6}$ )	0.343658-0.321024i ( $1.3 \times 10^{-6}, 3.4 \times 10^{-6}$ )
$Q = 1$	AIM ( $\xi = 0.45$ )	0.54590-0.34803i ( $6.2 \times 10^{-8}, -4.1 \times 10^{-7}$ )	1.198949-0.380392i ( $7.5 \times 10^{-6}, 1.6 \times 10^{-5}$ )
	CFM	0.54590-0.34803i ( $-1.4 \times 10^{-6}, 3.2 \times 10^{-7}$ )	1.198958-0.380398i ( $-1.7 \times 10^{-11}, 3.6 \times 10^{-11}$ )

Table 2: Convergence of CFM and AIM as parameters  $Q$  and  $q$  vary. When  $Q$  is small,  $Q = 0.1$  for example, results given by both of these two methods have high accuracy and agree quite well. However, when  $Q$  becomes large,  $Q = 1$  for example, the convergence of the two methods depends on the value of  $q$ . For small  $q$ ,  $q = 0.5$  for example, the speed of the convergence of the AIM is faster than that of the CFM. However, as  $q$  increases, the speed of the convergence of the AIM slows down, while the speed of the convergence of the CFM increases and becomes faster than that of the AIM.

We have made comparisons of these two methods in various situations, and the results are summarized in Table 3. The AIM and the CFM have little difference in the speed of convergence and accuracy for small  $Q$ . For large  $Q$  (but not larger than 1), the AIM converges faster than the CFM when  $q$  is small but when  $q$  is large we find that the CFM is a better way in computation. When  $Q$  is larger than 1, the CFM fails to converge and we can only rely on the AIM.

The speed of convergence	Small $Q$		large $Q$	
	AIM	CFM	AIM	CFM
Small $q$	Little difference		Faster	Slower
Large $q$	Little difference		Slower	Faster

Table 3: The speed of the convergence comparisons between the AIM and the CFM for calculating the overtone  $n = 1$  with various  $Q(Q \leq 1)$  and  $q$ .

Moreover, it is known from (24) that the speed of convergence of AIM is related to the position of the expansion point. When  $Q$  is small, the position of the expansion  $\xi$  lies in a large range to permit the convergence of the AIM. However as the increase of  $Q$ , the range of the allowed expansion point to accommodate convergence becomes narrower and the value of  $\xi$  needs to be taken smaller. We choose  $\xi = 0.45$  when  $Q \leq 1$  and  $\xi = 0.43$  when  $Q > 1$  in our calculation. See the Table 4 for the comparison. For  $Q > 1$ , fine tuning of the expansion point is needed to control the convergence of the

computation by using the AIM.

$l = 2, Q = 1.2, q = 2$	AIM ( $\xi = 0.45$ )	AIM ( $\xi = 0.43$ )
iterative steps	80	80
overtone $n = 2$ (relative error with respect to 100 steps)	1.695567-0.631905i $(-4.7 \times 10^{-5}, 3.3 \times 10^{-4})$	1.695564-0.631910i $(-3.9 \times 10^{-8}, 5.1 \times 10^{-7})$

Table 4: The dependence of the speed of the convergence in the AIM on different chosen positions of the expansion.

## 4 Numerical results

In this section we report the frequencies of the charged scalar perturbations in the stringy black holes with the change of the parameters, such as the charge of the black hole  $Q$ , the charge of the perturbing scalar field  $q$  and the angular momentum index  $l$ . We will analyze the numerical results to see their effects on the frequencies of the perturbation.

### 4.1 The fundamental modes

In this subsection, we study the frequencies of the fundamental modes of the charged scalar perturbations. In Table 5, we give the results for various  $Q$  and  $q$  when  $l = 0$ . We use both of the two highly precise methods to study the frequency domain of the perturbation, and find that they give consistent results when  $Q \leq 1$ . When  $Q > 1$ , for example  $Q = 1.2$  in our table, we find that the CFM fails to converge so that we can only rely on the AIM in the computation. This challenges the argument that CFM is the most accurate method in calculating the frequencies of perturbations [19]. In our computations, we fix the number of iterative steps to be 100 in the two methods.

We found that in all cases, the imaginary frequencies of the perturbations are negative, which indicate that there are no unstable modes of the charged scalar perturbation around the GHS black hole. When the black hole charge disappears, we recover the Schwarzschild black hole and the fundamental modes we get in this limit reproduces the result of the Schwarzschild black hole under the scalar perturbation. Fixing the charge of the perturbation field, we find that the perturbation presents more oscillations but decays faster with the increase of the black hole charge  $Q$ . Compared with the real part, the imaginary part of the frequency changes slower when we vary  $Q$  or  $q$ .

The objective pictures of the dependence of the real and imaginary parts of the frequencies on varying  $Q$  and  $q$  are shown in Fig.1. From the left panel, we see that for the fixed  $Q$ ,  $\omega_R$  increases linearly as  $q$  increases with a slope  $\sim \frac{1}{2}Q$ . We fitted the data and found that  $\omega_R \sim 0.079 + 0.493Qq$ .

$l = 0$	$Q = 0.1$	$Q = 0.5$	$Q = 1$	$Q = 1.2$
$q = 0$	0.11064-0.10493i	0.11562-0.10599i	0.13736-0.10961i	0.15948-0.11120i
$q = 0.5$	0.13026-0.10804i	0.21716-0.11732i	0.34938-0.12550i	0.42072-0.12873i
$q = 1$	0.15019-0.11070i	0.32485-0.12258i	0.57549-0.12942i	0.69534-0.13332i
$q = 1.5$	0.17044-0.11297i	0.43710-0.12495i	0.81000-0.12991i	0.97805-0.13401i
$q = 2$	0.19098-0.11491i	0.55260-0.12596i	1.04946-0.12948i	1.26577-0.13343i
$q = 2.5$	0.21180-0.11658i	0.67038-0.12634i	1.29192-0.12885i	1.55668-0.13252i
$q = 3$	0.23288-0.11800i	0.78977-0.12643i	1.53630-0.12827i	1.84974-0.13159i
$q = 4$	0.27578-0.12025i	1.03171-0.12630i	2.02853-0.12735i	2.43985-0.13001i
$q = 5$	0.31955-0.12188i	1.27626-0.12607i	2.52344-0.12673i	3.03318-0.12886i
$q = 6$	0.36409-0.12306i	1.52236-0.12587i	3.01986-0.12632i	3.62839-0.12803i
$q = 7$	0.40928-0.12392i	1.76944-0.12571i	3.51721-0.12603i	4.22478-0.12743i
$q = 8$	0.45505-0.12453i	2.01718-0.12559i	4.01517-0.12582i	4.82197-0.12698i
$q = 10$	0.54797-0.12528i	2.51392-0.12541i	5.01226-0.12555i	6.01789-0.12637i
$q = 12$	0.64236-0.12564i	3.01169-0.12530i	6.01027-0.12539i	7.21530-0.12581i

Table 5: Fundamental modes of the GHS BH when  $l = 0$ . The CFM and the AIM give the consistent result when  $Q \leq 1$ . However, when  $Q > 1$ ,  $q = 1.2$  in the table for example, the CFM fails to converge and at this time we can only rely on the AIM. The iteration steps in both methods are taken to be 100. The expansion point in the AIM is taken to be  $\xi = 0.43$ . For Schwarzschild BH ( $Q = 0$ ), the fundamental mode reads  $\omega = 0.11047 - 0.10487i$ .

The behavior of  $\omega_I$  is more complicated. From the right panel, we observe that when  $Q$  is small,  $Q = 0.1$  for example,  $|\omega_I|$  is a monotonically increasing function of  $q$ . However, when  $Q$  becomes large,  $|\omega_I|$  is no longer a monotonic function of  $q$ . With the increase of  $q$ ,  $|\omega_I|$  first increases and then after reaching a maximum value it begins to decrease. With the increase of  $Q$ , we find that the imaginary part of the perturbation becomes more negative when the perturbation is weakly charged, which indicates that in this case the black hole is more stable. When  $q$  becomes big enough,  $\omega_I$  converges to a constant no matter what values of  $Q$  one chooses.

We plot the effective potential in Fig.2 to give some intuitive understandings of the properties of the fundamental modes discussed above. We find that  $V_{eff} \rightarrow -\frac{q^2 Q^2}{4M^2}$  when  $r \rightarrow 2M$ , while  $V_{eff} \rightarrow 0$  when  $r \rightarrow \infty$ . When  $q = 1$ , the effective potential has a barrier for small  $Q$ . The barrier becomes lower and even disappears as  $Q$  increases. This implies that the perturbing wave can fall into the black hole more easily when  $Q$  becomes larger, which explains the faster decay of the weakly charged scalar perturbation with the increase of  $Q$  as shown in the right panel of Fig.1. On the other hand, near the horizon, the potential is more negative for larger  $Q$ , which tells us that the perturbation can have more momentum to fall into the black hole and explains the reason that the perturbing scalar can have faster oscillation in the decay when  $Q$  increases. This supports the observation in the right

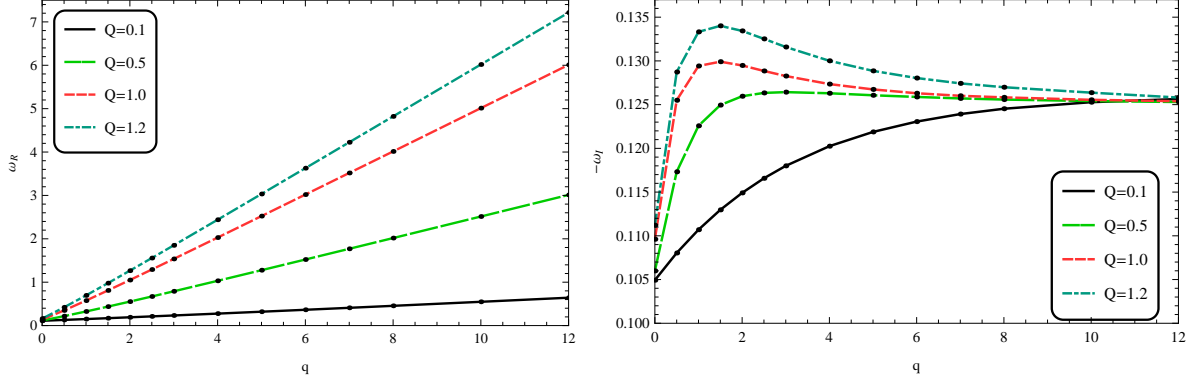


Figure 1: The fundamental modes of charged scalar perturbation of GHS BH when  $l = 0$ .

panel of Fig.1 that we have bigger real part of the perturbation frequency for bigger  $Q$ .

When  $q$  becomes large enough,  $q = 10$  for instance or even bigger, the potential barrier disappears for all  $Q$ . The perturbation wave can be absorbed by the black hole without any obstacles. This gives the same decay speed of the perturbation for all values of  $Q$  as shown in the right panel of Fig.1. On the other hand, at the black hole horizon, the differences in the potential values there caused by the black hole charge  $Q$  become bigger compared to the case with weakly charged scalar perturbation. This explains that the difference in the momentum for the perturbing wave to fall into the hole is enlarged when the scalar field is heavily charged, which explains the big difference in the real part of the frequency with the change of the black hole charge  $Q$  when the scalar perturbation is heavily charged as shown in the left panel of Fig.1.

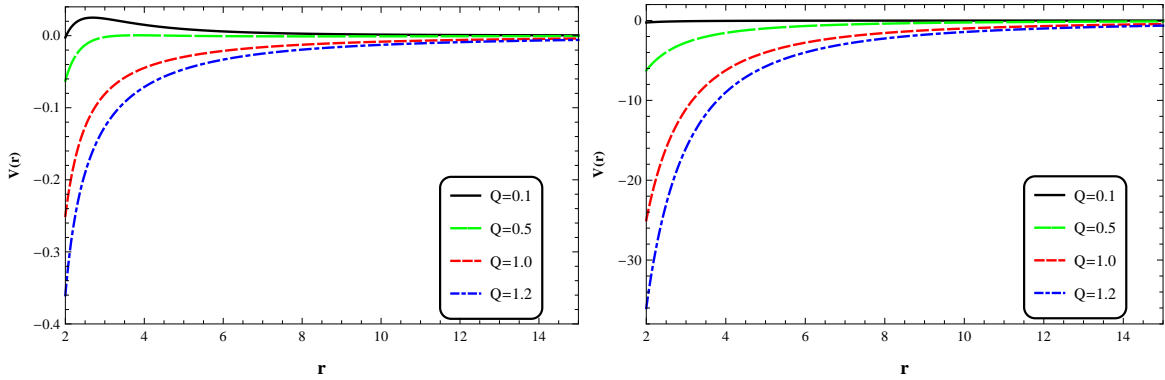


Figure 2: The effective potential for different  $Q$ s when  $l = 0$  (left for  $q = 1$ , right for  $q = 10$ ).

We also perform the same calculations for different angular indexes  $l = 1$  and  $l = 2$ , respectively, to

see the effect of the angular momentum. The results are listed in Table.6 and 7. The overall behaviors of the fundamental modes for  $l = 1$  and  $l = 2$  are similar to that of  $l = 0$ . Also, we can see that the imaginary part of the fundamental modes changes slowly while the real part changes significantly as we vary  $Q$  and  $q$ .

$l = 1$	$Q = 0.1$	$Q = 0.5$	$Q = 1$	$Q = 1.2$
$q = 0$	0.29343-0.09771i	0.30622-0.09899i	0.36304-0.10361i	0.42191-0.10624i
$q = 0.5$	0.31072-0.09940i	0.39622-0.10623i	0.55527-0.11470i	0.66341-0.11785i
$q = 1$	0.32829-0.10100i	0.49171-0.11158i	0.76093-0.12112i	0.91814-0.12457i
$q = 1.5$	0.34613-0.10250i	0.59173-0.11549i	0.97615-0.12478i	1.18197-0.12850i
$q = 2$	0.36422-0.10391i	0.69548-0.11833i	1.19842-0.12680i	1.45242-0.13075i
$q = 2.5$	0.38256-0.10524i	0.80232-0.12038i	1.42597-0.12785i	1.72788-0.13196i
$q = 3$	0.40113-0.10649i	0.91173-0.12185i	1.65756-0.12832i	2.00725-0.13252i
$q = 4$	0.43895-0.10877i	1.13661-0.12365i	2.12944-0.12842i	2.57463-0.13257i
$q = 5$	0.47761-0.11077i	1.36750-0.12457i	2.60924-0.12808i	3.15021-0.13200i
$q = 6$	0.51704-0.11254i	1.60265-0.12503i	3.09417-0.12766i	3.73137-0.13124i
$q = 7$	0.55718-0.11409i	1.84088-0.12525i	3.58258-0.12726i	4.31647-0.13048i
$q = 8$	0.59799-0.11544i	2.08137-0.12535i	4.07342-0.12692i	4.90445-0.12978i
$q = 10$	0.68138-0.11767i	2.56706-0.12538i	5.05994-0.12641i	6.08632-0.12865i
$q = 12$	0.76686-0.11938i	3.05688-0.12535i	6.05055-0.12606i	7.21341-0.12762i

Table 6: Fundamental modes of the GHS black hole with the angular index  $l = 1$ . The CFM and the AIM give the same results when  $Q \leq 1$ . However, when  $Q > 1$ ,  $q = 1.2$  in the table for example, the CFM fails to converge and so that we can only rely on the AIM. The iteration steps in the two methods are taken to be 100. The expansion point in the AIM is taken to be  $\xi = 0.43$ . For the limiting case ( $Q = 0$ ), we reproduce the result of the Schwarzschild black hole with the fundamental mode  $\omega = 0.29293 - 0.09766i$ .

In Fig.3, we plot the fundamental modes for different angular index  $l$  ( $l = 0, 1, 2$ ). From the figure, we can see that when  $Q$  is fixed, the real part of the frequency keeps linearly increasing with the increase of  $q$ , which is independent of the angular index  $l$ . For  $l = 1$ ,  $\omega_R \sim 0.252 + 0.481Qq$ . For  $l = 2$ ,  $\omega_R \sim 0.455 + 0.471Qq$ . Moreover, for fixed  $Q$ ,  $\omega_{RS}$  for different  $ls$  approach to each other as  $q$  becomes very large. This is even clearer when the black hole charge  $Q$  is large. As  $q$  increases, the imaginary part  $\omega_I$  flattens and approaches to constant values regardless of the chosen  $Q$  and  $l$ .

We plot the effective potential for different  $ls$  when  $Q = 0.5$  in Fig.4 to understand the curves in Fig.3 more intuitively. When  $q$  is small, the potential barrier increases as  $l$  increases. This means that the perturbing wave with higher  $l$  is more difficult to be absorbed into the black hole and decay so that its imaginary frequency is bigger. At the horizon, the potential drops faster when  $l$  is larger, thus for higher  $l$ , the perturbation falls into the black hole usually with bigger momentum so that it



can oscillate faster. At large  $q$ , the potential barriers disappear for all values of  $l$ . Furthermore, they basically coincide with each other for large  $q$  ( $q = 10$  for example in Fig.4). So both the real parts and the imaginary parts of the perturbation modes approach to each other at large  $q$ , as shown in Fig.3.

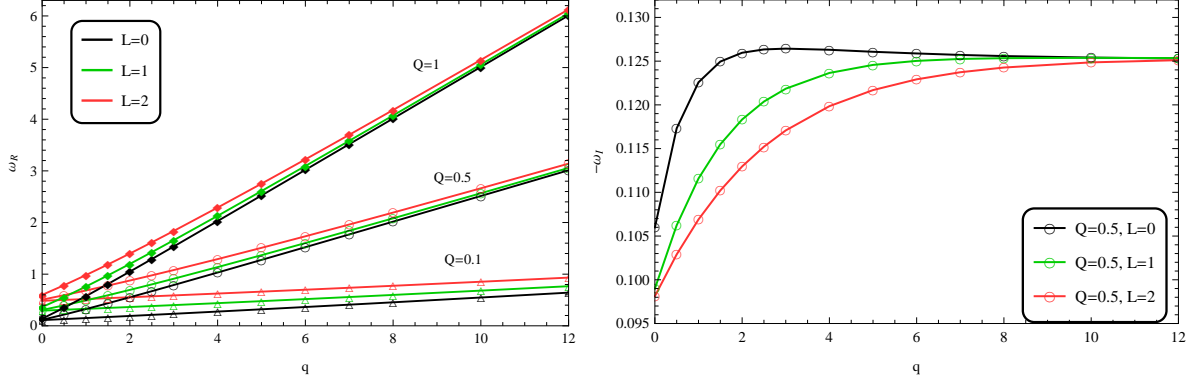


Figure 3: The fundamental modes of GHS BH for different  $l$ s and  $Q$ s (The first panel for real parts, the remaining panels for imaginary parts).

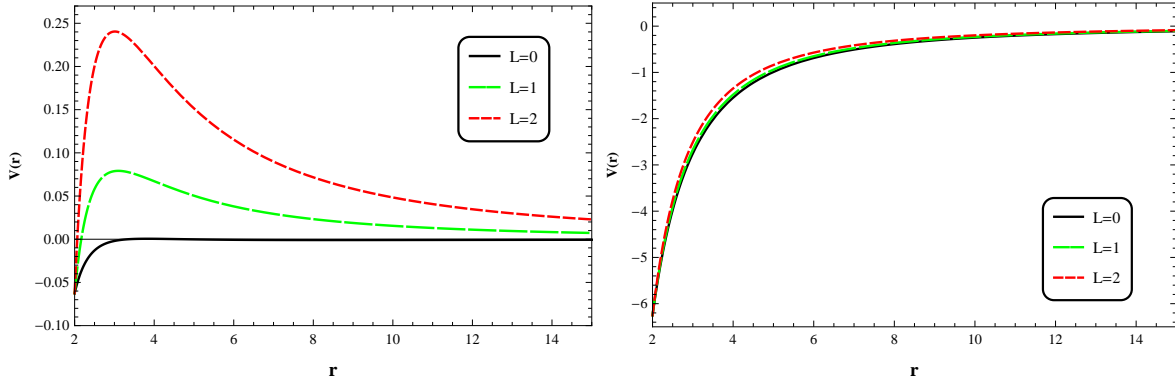


Figure 4: The effective potential for different  $l$ s when  $Q = 0.5$  (left for  $q = 1$ , right for  $q = 10$ ).

## 4.2 Overtones

Now we turn to present the results of the overtones of the charged scalar perturbation around the GHS black hole. We only list the fundamental modes and the first two overtones when  $l = 2$  in Table.7 for concision.

$l = 2$	overtones	$Q = 0.1$	$Q = 0.5$	$Q = 1$	$Q = 1.2$
$q = 0$	$n = 0$	0.48445-0.09681i	0.50541-0.09812i	0.59878-0.10291i	0.69577-0.10572i
	$n = 1$	0.46470-0.29575i	0.48660-0.29942i	0.58380-0.31271i	0.68476-0.32025i
	$n = 2$	0.43145-0.50876i	0.45489-0.51401i	0.55839-0.53288i	0.66619-0.54286i
$q = 2$	$n = 0$	0.55330-0.10086i	0.87667-0.11296i	1.39915-0.12269i	1.69259-0.12634i
	$n = 1$	0.53702-0.30696i	0.86989-0.34051i	1.39785-0.36838i	1.69356-0.37907i
	$n = 2$	0.50965-0.52437i	0.85816-0.57223i	1.39555-0.61487i	1.69556-0.63191i
$q = 4$	$n = 0$	0.62484-0.10437i	1.29143-0.11985i	2.28913-0.12753i	2.77507-0.13167i
	$n = 1$	0.61152-0.31664i	1.28926-0.35996i	2.28956-0.38258i	2.77690-0.39496i
	$n = 2$	0.58903-0.53793i	1.28531-0.60114i	2.29043-0.63758i	2.78057-0.65810i
$q = 6$	$n = 0$	0.69884-0.10739i	1.73335-0.12292i	3.22242-0.12824i	3.89915-0.13246i
	$n = 1$	0.68798-0.32498i	1.73272-0.36885i	3.22267-0.38472i	-
	$n = 2$	0.66956-0.54970i	1.73153-0.61501i	3.22316-0.64124i	-
$q = 8$	$n = 0$	0.77505-0.10998i	2.19246-0.12427i	4.17893-0.12791i	
	$n = 1$	0.76626-0.33215i	2.19230-0.37283i	4.17894-0.38374i	
	$n = 2$	0.75120-0.55992i	2.19200-0.62143i	4.17898-0.63962i	
$q = 10$	$n = 0$	0.85328-0.11220i	2.66269-0.12486i	5.14884-0.12741i	
	$n = 1$	0.84618-0.33831i	2.66267-0.37459i	5.14876-0.38224i	
	$n = 2$	0.83392-0.56879i	2.66262-0.62432i	5.14859-0.63710i	
$q = 12$	$n = 0$	0.93333-0.11409i	3.14034-0.12511i	6.12702-0.12696i	
	$n = 1$	0.92763-0.34359i	3.14034-0.37534i	6.12691-0.38089i	
	$n = 2$	0.91766-0.57647i	3.14036-0.62557i	6.12669-0.63482i	

Table 7: The frequencies of the charged scalar perturbations around the GHS black hole when  $l = 2$ . The CFM and the AIM give the same result when  $Q \leq 1$ . However, the CFM fails when  $Q > 1$ . The frequencies for  $Q = 1.2$  are calculated by the AIM. We adjust the expansion point to keep high precision and efficiency. The iteration step is 100. When  $Q = 1.2$  and  $q > 6$ , the precision of the results is lower than  $10^{-5}$  and the results are not shown in this table. For the Schwarzschild black hole ( $Q = 0$ ), the fundamental mode reads  $\omega = 0.48364 - 0.09675i$ .

It can be seen from Table.7 that when  $Q, q$  and  $l$  are fixed, the real parts of the overtones are nearly invariant while the imaginary parts change more significantly. To see more clearly, we plot the overtones for  $l = 1$  and  $l = 2$  in Fig. 5. We can see that the real part  $\omega_R$  is nearly independent of  $n$ , while the imaginary part  $\omega_I$  depends on  $n$  linearly. For example, when  $l = 1$ ,  $\omega_I$  can be approximated well by the form  $\omega_I \sim 0.1262 + 0.2562n$  when  $q = 6$  and  $\omega_I \sim 0.1261 + 0.2520n$  when  $q = 12$ . As  $q$  increases, the slope tends to 0.252. Meanwhile, the modes for different  $l$  also become closer to each other as  $q$  increases. This can be understood since the effective potential for different  $l$  approaches to each other when  $q$  is large.

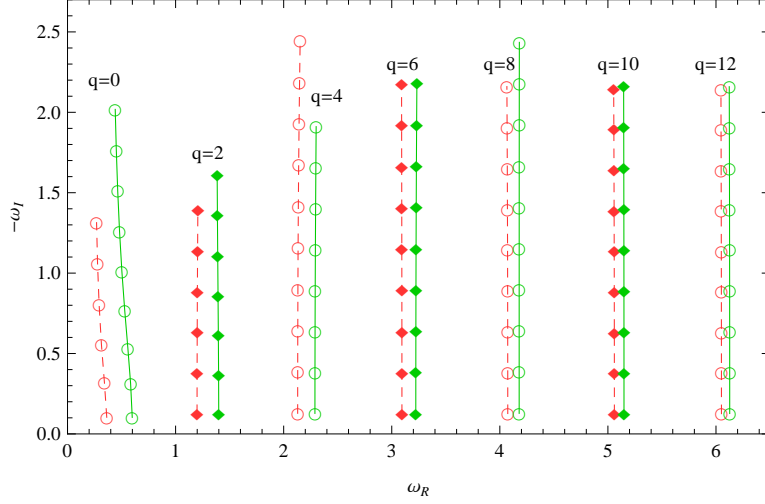


Figure 5: Overtones of perturbations around GHS black hole when  $Q = 1$ . The dashed left red line corresponds to the overtones when  $l = 1$  and the right green line corresponds to the overtones when  $l = 2$ .

### 4.3 The superradiance and its stability

In this subsection we will show that the superradiance with the amplification of the incident wave can not appear for the GHS black hole. We consider the classical scattering problem for a charged scalar field in the GHS black hole background.

The asymptotic behavior of (6) when  $\omega^2 > \mu^2$  can be derived straightforwardly,

$$\Psi \sim \begin{cases} T e^{-i(\omega - \frac{qQ}{2M})r_*}, & r_* \rightarrow -\infty (r \rightarrow 2M), \\ e^{-i\sqrt{\omega^2 - \mu^2}r_*} + B e^{i\sqrt{\omega^2 - \mu^2}r_*}, & r_* \rightarrow \infty (r \rightarrow \infty). \end{cases} \quad (29)$$

This boundary condition corresponds to an incident wave of unit amplitude from the infinity and a reflected wave of amplitude  $B$  back to the infinity and a transmitted wave of amplitude  $T$  towards the event horizon. Since the effective potential is real,  $\Psi^*$  is also a solution of the radial equation Eq. (6) and independent of  $\Psi$ . Thus, the Wronskian  $W \equiv \Psi \frac{d}{dr_*} \Psi^* - \Psi^* \frac{d}{dr_*} \Psi$  is independent of  $r_*$ . Calculating the Wronskian at the black hole horizon and at the infinity respectively, and equaling the two values, we get

$$1 - |B|^2 = \frac{\omega - \frac{qQ}{2M}}{\sqrt{\omega^2 - \mu^2}} |T|^2. \quad (30)$$

We see that if  $\mu < \omega < \frac{qQ}{2M}$ , the amplitude of the reflected wave is larger than the one of the incident wave  $|B|^2 > 1$ . This phenomenon is known as superradiance. Thus, we get the superradiance condition

$$\mu < \omega < \frac{qQ}{2M}. \quad (31)$$

This condition was also derived in [32, 33].

Multiplying the complex conjugated field  $\Psi^*$  on both sides of (6) and doing partial integration, we get

$$\Psi^*(r_*)\Psi'(r_*)|_{-\infty}^{\infty} + \int_{-\infty}^{\infty} (\omega - q\Phi)^2 |\Psi(r_*)|^2 dr_* = \int_{-\infty}^{\infty} (V|\Psi(r_*)|^2 + |\Psi'(r_*)|^2) dr_*, \quad (32)$$

in which  $\Phi = \frac{Q}{r}$ . Note that the right hand side of the above equation is real and positive since  $V$  is positive. Taking imaginary part of both sides, we get

$$(a^2 + b^2)^{\frac{1}{4}} \cos\left(\frac{1}{2} \arctan \frac{b}{a}\right) + \omega_R - q\Phi_h + \int_{-\infty}^{\infty} 2\omega_I (\omega_R - q\Phi) |\Psi(r_*)|^2 dr_* = 0. \quad (33)$$

Here we have taken notations  $\omega = \omega_R + i\omega_I$ ,  $a = \omega_R^2 - \omega_I^2 - \mu^2$ ,  $b = 2\omega_R\omega_I$  and  $\Phi_h = \frac{qQ}{2M}$ . Since  $\arctan \frac{b}{a} \in (-\frac{\pi}{2}, \frac{\pi}{2})$  and  $\Phi$  is a monotonic decreasing function, we get  $\omega_I < 0$  if  $\omega_R > q\Phi_h$ . Thus, if the instability with  $\omega_I > 0$  occurs, we must have  $\omega_R < q\Phi_h$ . This tells us that the instability can only take place when

$$\mu < \omega_R < q\Phi_h, \quad (34)$$

which is the superradiance condition Eq. (31). Thus if the GHS black hole experiences instability, this instability must be superradiant instability.

But from the above computations, we always find that the perturbation modes with  $\omega_R$  are beyond the superradiant condition Eq. (31), no matter what parameter ranges we choose. According to the analytical argument, these modes should be stable with  $\omega_I < 0$ , which are consistent with our numerical results above. On the other hand, from the effective potential, we do not see the potential well outside the black hole to accumulate the energy. The necessary condition for the existence of the superradiant instability does not hold. Thus the superradiant instability cannot exist in the GHS background.

## 5 Summary and discussion

In this paper, we have discussed the stability of the GHS black hole under charged scalar perturbations. For the charged scalar perturbations, we have found that not all available numerical methods can efficiently compute the accurate frequencies of the perturbations. This is different from that of the neutral scalar perturbations. We have discovered that two numerical methods, the CFM and the AIM, can still keep high accuracy and efficiency in the computations of the frequency of the charged scalar perturbations. We have experienced that the speed of convergence of the AIM depends on the position of the expansion point which needs to be chosen suitably. Besides, we have observed that the speed of convergence of CFM is close to that of the AIM when the black hole charge  $Q$  is small. However, when  $Q$  becomes large but still smaller than the mass of the black hole  $M$ , the AIM has faster convergence than the CFM when the scalar field is weakly charged; but the result is opposite when the charge of the scalar field is big. When the black hole charge  $Q$  exceeds the black hole mass  $M$ , the CFM is found invalid to give reliable results, while the AIM can still work. However, the convergence of the AIM becomes bad as  $Q$  approaches to the extremal value  $\sqrt{2}$ . The results have been summarized in Table 3. The comparisons of the efficiency and accuracy among different numerical methods are important, because the accuracy and convergence of the numerical computations are key requirements to grasp the properties in the perturbations around black holes.

The influences on the frequencies of the perturbations brought by parameters describing the background and the perturbation field have been illustrated. The intuitive reasons behind these phenomena have also been discussed. We have observed that the GHS black hole spacetime, which can reduce to the Schwarzschild black hole when the black hole charge goes to zero, is stable against the charged scalar perturbation. This result is different from what have been disclosed in the AdS black holes and the dS black holes with vanishing angular momentum, where the backgrounds experience instability under the charged scalar perturbations, while keep stable against neutral scalar perturbations.

In [7] it was concluded that the new instability in the dS black hole against charged scalar perturbations with vanishing angular momentum is caused by the superradiance. This was further confirmed in [8]. For the GHS black hole spacetime, we have shown that the superradiance does not happen. Recently the superradiant instability of the GHS background was discussed in [34, 35]. But they put the black hole in the artificial cavity. Although in this way they claimed that they can devise a black hole bomb, the mechanism with the artificial mirror is not convincing. One needs to introduce a natural wall, for example the massive fields [36, 37], to trigger the superradiant instability. It was proved in [32] that the reflecting mirror made by the mass term of the incident field cannot trigger the superradiant instability and create the GHS black hole bomb. Our result has further argued that the

GHS black hole background is always stable against the charged scalar perturbation. Considering that the incident charged scalar wave cannot be amplified due to the superradiance around the GHS hole and the property of the effective potential, we find that the superradiant instability cannot happen in the GHS black hole background.

## Acknowledgements

We thank E. Abdalla, Y.Q. Liu, Z.Y. Zhu and D.C. Zou for helpful discussions. This work was supported by NNSF of China.

## References

- [1] R. A. Konoplya and A. Zhidenko, Rev. Mod. Phys. **83**, 793 (2011) [arXiv:1102.4014 [gr-qc]].
- [2] B. Wang, Braz. J. Phys. **35**, 1029 (2005) [arXiv:gr-qc/0511133].
- [3] X. He, B. Wang, R. -G. Cai and C. -Y. Lin, Phys. Lett. B 688, 230 (2010) [arXiv:1002.2679].
- [4] E. Abdalla, C. E. Pellicer, J. de Oliveira and A. B. Pavan, Phys. Rev. D 82, 124033 (2010)[arXiv:1010.2806].
- [5] Y. Liu and B. Wang, Phys. Rev. D 85, 046011 (2012) [arXiv:1111.6729].
- [6] S. A. Hartnoll, Class. Quant. Grav. **26**, 224002 (2009) [arXiv:0903.3246 [hep-th]].
- [7] Z. Zhu, S. J. Zhang, C. E. Pellicer, B. Wang and E. Abdalla, Phys. Rev. D **90**, no. 4, 044042 (2014) [Addendum-ibid. D **90**, no. 4, 049904 (2014)] [arXiv:1405.4931 [hep-th]].
- [8] R. A. Konoplya and A. Zhidenko, Phys. Rev. D **90**, 064048 (2014) [arXiv:1406.0019 [hep-th]].
- [9] D. Garfinkle, G. T. Horowitz and A. Strominger, Phys. Rev. D **43**, 3140 (1991) [Erratum-ibid. D **45**, 3888 (1992)].
- [10] G. T. Horowitz, In \*Trieste 1992, Proceedings, String theory and quantum gravity '92\* 55-99 [hep-th/9210119].
- [11] S. Fernando, Gen. Rel. Grav. **36** (2004) 71 [arXiv:hep-th/0306214].  
S. Fernando, Phys. Rev. D **77** (2008) 124005 [arXiv:0802.3321 [hep-th]].  
A. López-Ortega, Gen. Rel. Grav. **37** (2005) 167.

- [12] R. Becar, S. Lepe and J. Saavedra, Phys. Rev. D **75** (2007) 084021 [arXiv:gr-qc/0701099].  
A. López-Ortega, Int. J. Mod. Phys. D **18**, 1441 (2009) [arXiv:0905.0073 [gr-qc]].  
R. Bécar, P. A. GonzBález and Y. VBásquez, Eur. Phys. J. C **74**, 3028 (2014) [arXiv:1404.6023 [gr-qc]].  
R. Bécar, P. A. GonzBález and Y. VBásquez, Eur. Phys. J. C **74**, 2940 (2014) [arXiv:1405.1509 [gr-qc]].
- [13] V. Ferrari, M. Pauri and F. Piazza, Phys. Rev. D **63**, 064009 (2001) [gr-qc/0005125].  
S. Fernando and K. Arnold, Gen. Rel. Grav. **36**, 1805 (2004) [hep-th/0312041].  
R. A. Konoplya, Phys. Rev. D **66**, 084007 (2002) [gr-qc/0207028].
- [14] E. W. Leaver, Proc. R. Soc. London **A402**, 285 (1985).  
E. W. Leaver, Phys. Rev. D **34**, 384 (1986);  
E. W. Leaver, J. Math. Phys. **27**, 1238 (1986).
- [15] E.W. Leaver, Phys. Rev. D, **41**, 2986-2997, (1990).
- [16] H. Ciftci, R. L. Hall, and N. Saad, J. Phys. A **36**, 11807-11816 (2003)  
H. Ciftci, R. L. Hall and N. Saad, Phys. Lett. A **340**, 388 (2005).
- [17] H. T. Cho, A. S. Cornell, J. Doukas and W. Naylor, Class. Quant. Grav. **27**, 155004 (2010) [arXiv:0912.2740 [gr-qc]].
- [18] H. T. Cho, A. S. Cornell, J. Doukas, T. R. Huang and W. Naylor, Adv. Math. Phys. **2012**, 281705 (2012) [arXiv:1111.5024 [gr-qc]].
- [19] E. Berti, V. Cardoso and A. O. Starinets, Class. Quant. Grav. **26**, 163001 (2009) [arXiv:0905.2975 [gr-qc]].
- [20] V. P. Frolov and I. D. Novikov, Black hole physics: Basic concepts and new developments , Dordrecht, Netherlands: Kluwer Academic (1998).
- [21] Y. Fujii and K. Maeda, Cambridge, USA: Univ. Pr. (2003) 240 p.  
V. Faraoni, Springer (2004) 274 p.
- [22] G. W. Gibbons and C. M. Hull, Phys. Lett. B **109**, 190 (1982).  
G. W. Gibbons and K. i. Maeda, Nucl. Phys. B **298**, 741 (1988).
- [23] T. Barakat, Int. J. Mod. Phys. A **21**, 4127 (2006).

- [24] S. Chandrasekhar, S. Detweiler, Proc. R. Soc. Lond. **A344**, 441-452 (1975).
- [25] C. Molina, P. Pani, V. Cardoso and L. Gualtieri, Phys. Rev. D **81**, 124021 (2010) [arXiv:1004.4007 [gr-qc]].
- [26] B. F. Schutz and C. M. Will, Astrophys. J. **L291**, 33 (1985).
- [27] S. Iyer and C. M. Will, Phys. Rev. D **35**, 3621 (1987).
- [28] R. A. Konoplya, Phys. Rev. D **68**, 124017 (2003) [arXiv:hep-th/0309030].  
R. A. Konoplya, J. Phys. Stud. **8**, 93 (2004).
- [29] C. Gundlach, R. H. Price and J. Pullin, Phys. Rev. D **49**, 883 (1994) [arXiv:gr-qc/9307009].  
C. Gundlach, R. H. Price and J. Pullin, Phys. Rev. D **49**, 890 (1994) [arXiv:gr-qc/9307010].
- [30] B. Wang, C. Y. Lin and C. Molina, Phys. Rev. D **70**, 064025 (2004) [arXiv:hep-th/0407024].
- [31] E. Berti, V. Cardoso, J. A. Gonzalez and U. Sperhake, Phys. Rev. D **75**, 124017 (2007) [arXiv:gr-qc/0701086].
- [32] R. Li, Phys. Rev. D **88**, 127901 (2013) [arXiv:1310.3587 [gr-qc]].
- [33] K. Shiraishi, Mod. Phys. Lett. A **7**, 3449 (1992);  
J. Koga and K. Maeda, Phys. Lett. B **340**, 29 (1994).
- [34] R. Li and J. Zhao, Eur. Phys. J. C **74**, 3051 (2014) [arXiv:1403.7279 [gr-qc]].
- [35] R. Li and J. Zhao, Phys. Lett. B **12**, 007. (2014). [arXiv:1412.1527 [gr-qc]].
- [36] S. Hod, Phys. Lett. B **718** (2013) 1489; S. Hod, Phys. Lett. B **713** (2012) 505.
- [37] S. J. Zhang, B. Wang and E. Abdalla, arXiv:1306.0932 [gr-qc].